Published in final edited form as:
Heart Rhythm. 2013 August ; 10(8): 1109–1116. doi:10.1016/j.hrthm.2013.04.015.

Feasibility of Image-Based Simulation to Estimate Ablation Target in Human Ventricular Arrhythmia

Hiroshi Ashikaga, MD, PhD[1,2], **Hermenegild Arevalo, MS**[2,3], **Fijoy Vadakkumpadan, PhD**[2,3], **Robert C. Blake III, MCS**[2,3], **Jason D. Bayer, MS**[2,3], **Saman Nazarian, MD, PhD**[1], **M. Muz Zviman, PhD**[1], **Harikrishna Tandri, MD**[1], **Ronald D. Berger, MD, PhD**[1], **Hugh Calkins, MD**[1], **Daniel A. Herzka, PhD**[2], **Natalia A. Trayanova, PhD**[2,3], and **Henry R. Halperin, MD, MA**[1,2,4]

[1]Division of Cardiology, Johns Hopkins University School of Medicine

[2]Department of Biomedical Engineering, Johns Hopkins University School of Medicine

[3]Institute for Computational Medicine, Johns Hopkins University

[4]The Russell H. Morgan Department of Radiology and Radiological Sciences, Johns Hopkins University School of Medicine

Abstract

Background—Previous studies suggest that MRI with late gadolinium enhancement (LGE) may identify slowly conducting tissues in scar-related ventricular tachycardia (VT).

Objective—We tested the feasibility of image-based simulation based on LGE to estimate ablation targets in VT.

Methods—We conducted a retrospective study in 13 patients who had pre-ablation MRI for scar-related VT ablation. We used image-based simulation to induce VT and estimate target regions according to the simulated VT circuit. The estimated target regions were co-registered with the LGE scar map and the ablation sites from the electroanatomical map in the standard ablation approach.

Results—In image-based simulation, VT was inducible in 12 patients (92.3%). All VTs showed macro-reentrant propagation patterns, and the narrowest width of estimated target region that an ablation line should span to prevent VT recurrence was 5.0 ± 3.4 mm. Out of 11 patients who underwent ablation, the results of image-based simulation and the standard approach were consistent in 9 patients (82%), where ablation within the estimated target region was associated with acute success (n=8) and ablation outside the estimated target region was associated with failure (n=1). In one case (9%), the results of image-based simulation and the standard approach were inconsistent, where ablation outside the estimated target region was associated with acute success.

Address of Correspondence: Hiroshi Ashikaga, MD, PhD, Cardiac Arrhythmia Service, Division of Cardiology, Johns Hopkins University School of Medicine, 600 N. Wolfe Street, Carnegie 568, Baltimore, MD 21287, Phone 410-502-7861| Fax 410-502-0231| hashika1@jhmi.edu.

Disclosures: A part of the present study was presented at the Melvin Judkins Young Investigator Award Competition in 2011 Scientific Sessions of the American Heart Association in Orlando, FL. Drs Trayanova and Blake are members of the scientific advisory board of CardioSolv, LLC. This study was not supported by CardioSolv, LLC. The other authors report no competing financial interests.

Conclusions—The image-based simulation can be used to estimate potential ablation targets of scar-related VT. The image-based simulation may be a powerful noninvasive tool for pre-procedural planning of ablation procedures to potentially reduce the procedure time and complication rates.

Keywords

Image-guided intervention; Ventricular arrhythmia; Catheter ablation; Cardiac MRI; Computer simulation

Introduction

Scar-related ventricular tachycardia (VT) most commonly results from healed myocardial infarction (MI), and is frequently refractory to medical therapy. Perpetuation of VT critically depends on regions of relatively slow conduction of the impulse that allows other segments of the heart to recover excitability[1, 2]. The current approach of therapeutic ablation is to use invasive catheters to 'search and destroy' this slowly conducting tissue. However, this approach is time-consuming and often inaccurate, because VT cannot always be inducible during electrophysiology study (EPS), and it may be hemodynamically unstable. These limitations result in long procedure time, high complications rates and high recurrence rates[3–5].

Previous studies suggest that MRI with late gadolinium enhancement (LGE) may identify these slowly conducting tissues. The heterogeneous zone (HZ), defined as a highly complex mixture of scar and normal-appearing tissue in transition between the scar and the preserved normal tissues, is a structural basis of slowly conducting tissue[1, 6]. The HZ is commonly found in the infarct border zone. We have previously demonstrated that 1) MRI with LGE can identify the HZ, 2) LGE-derived HZ contains regions of abnormal electrical conduction, represented by fractionated electrograms, which are standard targets for ablation, 3) HZ can be found in the pathway within the VT circuit, and 4) Successful VT ablation targets are localized within the HZ, and incomplete ablation of the HZ is associated with recurrence[7–9]. Others also found that the LGE-derived HZ volume is a clinical predictor of VT and death[10–12].

Based on these results, we hypothesized that the HZ identified noninvasively by LGE contains the slowly conducting tissue that is the critical part of the VT circuits. To identify the critical components of the HZ that participate in the VT circuits, we can utilize a patient-specific, image-based computational simulation. We conducted a retrospective study to evaluate the feasibility of image-based simulation to estimate the potential ablation targets in scar-related VT.

Methods

The study workflow is shown in Figure 1. This study was retrospective but was conducted in a double-blind fashion, where the procedure operators were blinded to the simulation results, and those who performed image processing and simulation were blinded to the clinical results. Please refer to the Online Supplement for the detailed Methods.

Study Population

We retrospectively evaluated the patients who were referred for catheter ablation of VT between July 2006 and April 2011. Patients were included if the pre-ablation MRI with LGE showed myocardial scar, and were excluded if the pre-ablation MRI showed any artifacts within the heart from an implantable cardioverter defibrillator (ICD) and/or the ICD leads.

The patients underwent cardiac MRI with LGE with a 1.5-Tesla scanner[10] (Avanto, Siemens Medical Solutions).

Electrophysiology Study and Ablation

The patients underwent the standard EPS and ablation of scar-related VT under the guidance of three-dimensional (3-D) electroanatomical mapping system (CARTO, Biosense Webster, Diamond Bar, California). The standard substrate modification with radiofrequency (RF) ablation was performed during sinus rhythm. After ablation, programmed stimulation was repeated. Acute success was defined as inability to induce clinical VT at the end of the procedure. If non-clinical VT morphologies were inducible, those were also ablated.

Image Processing

A finite element mesh of the heart was created from the LGE images for computer simulation. The scar was defined as the myocardium with SI>50% of the maximal SI within the myocardium, and HZ was defined as the myocardium with SI>peak SI in the remote normal myocardium but <50% of maximal SI within the myocardium[10]. Myofiber orientation in the ventricles was estimated based on a modification of a rule-based method[13] where the transmural myofiber direction was assigned as a linear function of the distance from the endocardium to the epicardium, from +60° to −60°, respectively, with reference to the circumferential direction[14] (Figure 1). The transmural myolaminar sheet direction was fixed at −30° with reference to the radial direction[15].

Computer Simulation

We used a biophysically detailed model of whole heart electrophysiology to simulate VT. Ventricular tissue was modeled as monodomain, and the passive tissue properties anisotropic. The scar was modeled as an insulator. Membrane kinetics of the non-infarct tissue was represented by the ten Tusscher model of the human ventricular tissue[16]. The same membrane model was also modified to represent the electrophysiology of HZ cells. All simulations were performed using the software package CARP (CardioSolv, LLC) on a parallel computing platform, a 2,000-core Linux cluster; the numerical methodology has been described in previous publications[17–19]. A 500 millisecond-episode of activity in the multiscale monodomain model with a grid of 5.4 million elements typically took 3 hours to run on 15 nodes.

Statistical analysis

Continuous variables are presented as means ± SD, and categorical variables as numbers and percentages. Student's paired t-tests were performed to compare the extent of the estimated target region. A P value<0.05 is considered statistically significant. Statistical analysis was performed using Matlab (Statistical Toolbox, MathWorks, Inc, Natick, MA).

Results

Patients

In 34 patients referred for catheter ablation of VT, pre-ablation MRI with LGE showed myocardial scar. Twenty-one patients (61.8%) were excluded because of the presence of image artifact within the heart, regardless of the size and the location, resulting from an ICD and/or the ICD leads. The remaining 13 patients (38.2%) were included for analysis (Table 1). The age was 65 ± 9 years, and the left ventricular ejection fraction (LVEF) was 42 ± 16 %. Two patients (15.4%) were female, and two patients (15.4%) had an ICD. Nine patients (69.2%) had underlying coronary artery disease (CAD). All patients (n=13) underwent pre-ablation MRI and an electrophysiology study (EPS). Pre-ablation MRI showed the infarct

size was 24 ± 15 % of the LV myocardium (scar 11 ± 7 % and HZ 13 ± 10 %). The HZ size was 54 ± 19 % of the infarct. Pre-ablation MRI was performed 100 ± 285 days before the EPS (range 0 – 1041 days).

Standard approach

All patients had one clinical VT morphology, and the 12-lead ECG of clinical VT was available for all the cases prior to the EPS. The number of inducible VT morphologies at the time of EPS was 2 ± 1 (range 1 – 4, Table 1). The clinical VT morphology was inducible in all patients. All VT morphologies were hemodynamically unstable, therefore ablation was performed during sinus rhythm in all the cases. Catheter ablation was performed in 11 patients (84.6%), of which acute success was achieved in 10 patients (90.9%). The extent of ablation lesions was recorded in a 3-D electroanatomical map. The remaining two patients (15.4%) underwent the EPS without catheter ablation. The procedure time was 393 ± 152 minutes.

Image-based simulation

VT was inducible in image-based simulation in 12 patients (92.3%) (Supplemental Video 1–12). All inducible VTs showed macro-reentrant propagation patterns (Table 2). VT circuits were analyzed to identify the critical pathway segments circumscribed by lines of conduction block.

In 5 patients, the circuits were of the figure-of-eight reentry pattern, where two counter-rotating waves coexist at a relatively short distance from each other. The central common pathway, or the isthmus, of the two counter-rotating waves was located over the HZ or the superficial layer of viable myocardium over the scar. In this type of circuit, the target region was estimated to be an area bordered by two facing lines of conduction block that compose the isthmus (green area, "*Simulation*"). An ablation line that spans between the two facing lines of conduction block is expected to prevent VT recurrence, and the minimum length of this hypothetical ablation line (i.e. narrowest isthmus width) was quantified.

In 7 patients, the circuits were of the unidirectional circus movement reentry pattern. In this type of circuit, the target region was estimated to be a triangular area that connects one end of the line of conduction block that is closer to an adjacent anatomical barrier (e.g. mitral annulus). An ablation line that extends the existing line of conduction block to the anatomical barrier is expected to prevent VT recurrence, and the minimum length of this hypothetical ablation line was quantified.

In one patient (7.7%), VT was not inducible in simulation. This case was a repeat ablation where the patient had undergone a previous ablation attempt for a focal, non-scar-related VT (Supplemental Figure 1c).

Comparison

The comparison between the image-based simulation and the standard approach was available in 10 patients. For example, Patient 3 (Figure 2a) had a large inferior MI ("*MRI*"). The simulation showed propagation of excitation wavefronts through the figure-of-eight reentry circuit over the basal inferior region, where electrical activation spread longitudinally over the isthmus toward the base, split into two opposite lateral directions, then returned longitudinally and apically to the other end of the isthmus (green arrows, "*Simulation*"). Simulation estimated that the potential target region to be the isthmus bordered by the two facing lines of conduction block in the endocardial viable layer in the basal inferior region (green area, "*Estimated target region*"). The narrowest width of the isthmus was 1.7 mm. This VT circuit was consistent with the 12-lead ECG of the clinical

VT induced in the EPS ("*Electrophysiology study*"). Co-registration of the CARTO map ("*Ablation*") and simulation demonstrates that most of the RF ablation lesions fell within the estimated target region (yellow circles, "*Estimated target region"*). In this case, the results of image-based simulation and the standard approach were determined to be consistent.

Patient 6 (Figure 4b) had a large area of scar and HZ in the septum due to cardiac sarcoidosis ("*MRI*"). Simulation showed a unidirectional circus movement reentry (green arrows, "*Simulation*") and the target region was estimated to be a triangular area that connects the superior end of the line of conduction block to the mitral annulus (green area, "*Estimated target region"*). This area was located in the superficial viable layer over the scar in the posterior septum. Three ablation lesions fell in the estimated target region (yellow circles, "*Estimated target region"*). These lesions do not appear to span the target region by themselves. However, because one end of the line of conduction block was relatively close to the mitral annulus (minimum length = 5.7 mm), and each ablation usually creates lesions of at least 5–6 mm in diameter, these three lesions likely created a line of block with ablation in the target region (green area, "*Estimated target region"*).

Patient 11 (Supplemental Figure 2) had an MI in the lateral apex ("*MRI*"). In simulation, the line of conduction block was located in the apical border of the MI (blue line, "*Simulation*" and "*MRI*"). The target region was estimated to be a triangular area that connects the posterior end of the line of conduction block to the mitral annulus (green area, "*Estimated target region"*). This area was located in the viable layer over the posterior border of the MI. Only one ablation lesion fell in the estimated target region (yellow circle, "*Estimated target region"*), and the minimum length of possible ablation line was relatively long (= 9.7 mm). Thus, it is unlikely that this ablation lesion created a line of block in the target region (green area, "*Estimated target region"*). In fact, this case did not achieve acute success by the standard approach. Therefore the results of the image-based simulation and the standard approach were determined to be consistent.

Patient 13 (Figure 3c) had an extensive MI in the septum and the inferior region ("*MRI*"). In simulation, the target region was estimated to be a triangular area that connects the superior end of the line of conduction block to the mitral annulus (green area, "*Estimated target region"*). This area was located in the superficial viable layer over the scar in the posterior septum. Multiple ablation lesions were created in the standard approach, but none fell in the estimated target region (dashed red circles, "*Estimated target region"*). However, clinically this case achieved acute success. In this case, the results of the image-based simulation and the standard approach were determined to be inconsistent.

In summary, 1) Based on image-based simulation, the narrowest width of target region that an ablation line should span to prevent VT recurrence was 5.0 ± 3.4 mm, 2) In 9 out of 11 cases (82%), the results of the image-based simulation and the standard approach were consistent, where ablation within the estimated target region was associated with acute success (n=8) and ablation outside the estimated target region was associated with failure (n=1), 3) In one case (9%), VT was not inducible in simulation. This case was a repeat ablation where the patient had undergone a previous ablation attempt for a focal, non-scar-related VT, 4) In one case (9%), the results of the image-based simulation and the standard approach were inconsistent, where ablation outside the estimated target region was associated with acute success. The results are summarized in Table 2.

Discussion

Image-based simulation in electrophysiology has been used in animal models[20–23], but this is the first study to apply the image-based simulation to reproduction of clinical arrhythmia and estimation of ablation targets in human patients.

Feasibility

The comparison between the image-based simulation and the standard approach showed that these two approaches are highly consistent with each other (82%, Table 2). This indicates that image-based simulation can be used to estimate potential ablation targets. Our simulation results indicate that the narrowest width of the of target region that an ablation line should span to prevent VT recurrence was relatively small (5.0 ± 3.4 mm, Table 2). Pre-procedural estimation of the location and the size of the target region by image-based simulation would likely help reduce the procedure time.

In this study, ablation was performed on the LV endocardium and achieved acute success in 91% of the cases. However, in most cases the target region was estimated to reside on the opposite side of the wall, including the LV epicardium or the RV septum. There are possible mechanisms to explain this apparently contradictory result.

One possible explanation is that the lines of conduction block and the target regions are in fact 3-D structures within the myocardium, and ablation on the LV endocardium may have destroyed the hidden target region in the mid-myocardium. Furthermore, some lines or surfaces of conduction block may purely be a mid-myocardial structure hidden from both the endocardial and the epicardial surfaces. Such mid-myocardial structure can create target regions in the mid-myocardium. This may account for the case of Patient 13 (Figure 3c) where the image-based simulation and the standard approach showed inconsistent results. In this case, acute success was achieved but ablation was outside the target regions estimated from VT circuits on the heart surfaces. These ablation sites may have destroyed the hidden mid-myocardial target region that is not evident from the heart surfaces. In fact, the scar and the HZ in the septum in this patient were mostly in the mid-myocardium. This explains why the endocardial voltage map of most of the VT circuit region shows normal voltage (= pink, "*Ablation*").

Another explanation is that, although ablation was performed from the opposite side of the wall, it created sufficiently large physical disruption of the myocardial tissue for acute success. For example, a standard 3.5-mm tip, open-irrigation ablation catheter used in most of the cases can create a spherical lesion of as large as 5–6 mm in diameter.

Mechanistic implications

Contrary to our hypothesis, we found that the slowly conducting tissue that is the critical part of the reentry VT circuits was not limited to the HZ but also localized in the superficial rim of the scar. This result is indeed consistent with our previous report that demonstrated the isthmus of the reentry VT circuits was located either within the HZ or over the superficial rim of the scar[7]. The mechanism of slow conduction in the superficial rim of the scar is likely due to a sudden increase in the convexity of the electrical wavefront curvature and the resulting impedance mismatch caused by sharp scar thickness transition at the infarct border zone[24]. These findings highlight the utility of image-based simulation because the critical part of the reentry VT circuits was not intuitively identifiable by simply reviewing the MR images with scar and HZ tissues in our cases.

Comparison with other advanced mapping systems

The advantage of our image-based simulation system is that it is completely noninvasive, whereas the standard contact (e.g. CARTO [Biosense Webster], NavX [St. Jude]), non-contact (EnSite [St. Jude]) electroanatomical mapping systems and the multi-electrode basket catheter system (Constellation [Boston Scientific]) require invasive catheter insertion at the time of the electrophysiology study. The noninvasive nature of our system allows pre-procedural diagnosis and planning of ablation. Our system provides complementary advantages over ECG imaging (CardioInsight)[25], which is another advanced noninvasive mapping system that has been gathering attention. An advantage of our technique over ECG imaging is that the target arrhythmia does not necessarily need to be inducible at the time of pre-procedure planning or at the invasive electrophysiology study, because the targets can be identified in simulation. This advantage would address therapeutic approaches to the arrhythmias which tend to become nonunducible due to sedation or general anesthesia at the time of the electrophysiology study.

Limitations

Despite promising results, in this small feasibility study the accuracy of target estimation could not precisely be quantified, because it was not possible to retrospectively determine which ablation lesion(s) was critical in preventing VT recurrence. The patients were highly selected and the sample size was small. However, the study participants represent the prototypical patient population who are referred for scar-related VT ablation (Table 1)[3]. Because tissue properties in LGE were used as a surrogate for electrical properties of the myocardium, the image-based simulation is not applicable to idiopathic VT, or ventricular arrhythmias without distinct scar identified by LGE. Because all the VTs were hemodynamically unstable, we were not able to validate the simulated VT circuits against the activation maps from the patients. Due to a difficulty in acquiring myofiber orientation in human *in vivo*, we used estimated myofiber orientation based on ventricular geometry in the assembly of patient-specific computer simulation. Because myofiber orientation within the non-scar myocardium is preserved during the progression of ventricular remodeling[26], estimated myofiber orientation seems to be sufficient to estimate the location of target regions in this patient population.

Conclusion

Image-based simulation can be used to estimate potential ablation targets of scar-related VT. Image-based simulation may be a powerful noninvasive tool for pre-procedural planning of ablation procedures to potentially reduce the procedure time and complication rates.

Supplementary Material

Refer to Web version on PubMed Central for supplementary material.

Acknowledgments

Sources of Funding: NIH R01-HL094610 (to H.R.H.) and R01-HL082729 (to N.A.T.).

We thank Rozann Hansford for excellent patient care and monitoring during pre-ablation MRI scanning. We also thank Bernadette Barcelon for management of the patient database.

Glossary of Abbreviations

CAD	Coronary artery disease

CFD	Computational fluid dynamics
VT	Ventricular tachycardia
MI	Myocardial infarction
HZ	Heterogeneous zone
LGE	Late gadolinium enhancement
ICD	Implantable cardioverter defibrillator
Gd-DTPA	Gadolinium diethylenetriaminepentacetate
GRE	Gradient echo
LV	Left ventricle/ventricular
RV	Right ventricle/ventricular
3-D	Three-dimensional
RF	Radiofrequency
SI	Signal intensity
EPS	Electrophysiology study
LVAD	Left ventricular assist device
PES	Programmed electrical stimulation

References

1. de Bakker JM, van Capelle FJ, Janse MJ, et al. Reentry as a cause of ventricular tachycardia in patients with chronic ischemic heart disease: electrophysiologic and anatomic correlation. Circulation. 1988; 77:589–606. [PubMed: 3342490]
2. Stevenson WG, Khan H, Sager P, et al. Identification of reentry circuit sites during catheter mapping and radiofrequency ablation of ventricular tachycardia late after myocardial infarction. Circulation. 1993; 88:1647–1670. [PubMed: 8403311]
3. Stevenson WG, Wilber DJ, Natale A, et al. Irrigated radiofrequency catheter ablation guided by electroanatomic mapping for recurrent ventricular tachycardia after myocardial infarction: the multicenter thermocool ventricular tachycardia ablation trial. Circulation. 2008; 118:2773–2782. [PubMed: 19064682]
4. Tanner H, Hindricks G, Volkmer M, et al. Catheter ablation of recurrent scar-related ventricular tachycardia using electroanatomical mapping and irrigated ablation technology: results of the prospective multicenter Euro-VT-study. Journal of cardiovascular electrophysiology. 2010; 21:47–53. [PubMed: 19656251]
5. Calkins H, Epstein A, Packer D, et al. Catheter ablation of ventricular tachycardia in patients with structural heart disease using cooled radiofrequency energy: results of a prospective multicenter study. Cooled RF Multi Center Investigators Group. Journal of the American College of Cardiology. 2000; 35:1905–1914. [PubMed: 10841242]
6. Karagueuzian HS, Fenoglio JJ Jr, Weiss MB, Wit AL. Protracted ventricular tachycardia induced by premature stimulation of the canine heart after coronary artery occlusion and reperfusion. Circulation research. 1979; 44:833–846. [PubMed: 428076]
7. Ashikaga H, Sasano T, Dong J, et al. Magnetic resonance-based anatomical analysis of scar-related ventricular tachycardia: implications for catheter ablation. Circulation research. 2007; 101:939–947. [PubMed: 17916777]
8. Ashikaga H, Mickelsen SR, Ennis DB, et al. Electromechanical analysis of infarct border zone in chronic myocardial infarction. American journal of physiology. 2005

9. Estner HL, Herzka DA, Castro V, et al. Heterogeneous zones in magnet resonance images are the critical areas for ventricular tachycardia and for successful ablation. Circulation. 2009; 120:S690.
10. Schmidt A, Azevedo CF, Cheng A, et al. Infarct tissue heterogeneity by magnetic resonance imaging identifies enhanced cardiac arrhythmia susceptibility in patients with left ventricular dysfunction. Circulation. 2007; 115:2006–2014. [PubMed: 17389270]
11. Yan AT, Shayne AJ, Brown KA, et al. Characterization of the peri-infarct zone by contrast-enhanced cardiac magnetic resonance imaging is a powerful predictor of post-myocardial infarction mortality. Circulation. 2006; 114:32–39. [PubMed: 16801462]
12. Roes SD, Borleffs CJ, van der Geest RJ, et al. Infarct tissue heterogeneity assessed with contrast-enhanced MRI predicts spontaneous ventricular arrhythmia in patients with ischemic cardiomyopathy and implantable cardioverter-defibrillator. Circulation Cardiovascular imaging. 2009; 2:183–190. [PubMed: 19808591]
13. Bayer JD, Blake RC, Plank G, Trayanova NA. A Novel Rule-Based Algorithm for Assigning Myocardial Fiber Orientation to Computational Heart Models. Annals of biomedical engineering. 2012
14. Streeter DD Jr, Spotnitz HM, Patel DP, Ross J Jr, Sonnenblick EH. Fiber orientation in the canine left ventricle during diastole and systole. Circulation research. 1969; 24:339–347. [PubMed: 5766515]
15. LeGrice IJ, Smaill BH, Chai LZ, Edgar SG, Gavin JB, Hunter PJ. Laminar structure of the heart: ventricular myocyte arrangement and connective tissue architecture in the dog. The American journal of physiology. 1995; 269:H571–582. [PubMed: 7653621]
16. ten Tusscher KH, Noble D, Noble PJ, Panfilov AV. A model for human ventricular tissue. American journal of physiology. 2004; 286:H1573–1589. [PubMed: 14656705]
17. Plank G, Zhou L, Greenstein JL, et al. From mitochondrial ion channels to arrhythmias in the heart: computational techniques to bridge the spatio-temporal scales. Philosophical transactions. 2008; 366:3381–3409. [PubMed: 18603526]
18. Vigmond EJ, Hughes M, Plank G, Leon LJ. Computational tools for modeling electrical activity in cardiac tissue. Journal of electrocardiology. 2003; 36 (Suppl):69–74. [PubMed: 14716595]
19. Vigmond EJ, Weber dos Santos R, Prassl AJ, Deo M, Plank G. Solvers for the cardiac bidomain equations. Progress in biophysics and molecular biology. 2008; 96:3–18. [PubMed: 17900668]
20. Ng J, Jacobson JT, Ng JK, et al. Virtual electrophysiological study in a 3-dimensional cardiac magnetic resonance imaging model of porcine myocardial infarction. Journal of the American College of Cardiology. 2012; 60:423–430. [PubMed: 22633654]
21. Pop M, Sermesant M, Liu G, et al. Construction of 3D MR image-based computer models of pathologic hearts, augmented with histology and optical fluorescence imaging to characterize action potential propagation. Medical image analysis. 2012; 16:505–523. [PubMed: 22209561]
22. Vigmond E, Vadakkumpadan F, Gurev V, et al. Towards predictive modelling of the electrophysiology of the heart. Experimental physiology. 2009; 94:563–577. [PubMed: 19270037]
23. Vadakkumpadan F, Rantner LJ, Tice B, et al. Image-based models of cardiac structure with applications in arrhythmia and defibrillation studies. Journal of electrocardiology. 2009; 42:157 e151–110. [PubMed: 19181330]
24. Ciaccio EJ, Ashikaga H, Kaba RA, et al. Model of reentrant ventricular tachycardia based on infarct border zone geometry predicts reentrant circuit features as determined by activation mapping. Heart Rhythm. 2007; 4:1034–1045. [PubMed: 17675078]
25. Wang Y, Cuculich PS, Zhang J, et al. Noninvasive electroanatomic mapping of human ventricular arrhythmias with electrocardiographic imaging. Science translational medicine. 2011; 3:98ra84.
26. Ashikaga H, Omens JH, Covell JW. Time-dependent remodeling of transmural architecture underlying abnormal ventricular geometry in chronic volume overload heart failure. American journal of physiology. 2004; 287:H1994–2002. [PubMed: 15242833]

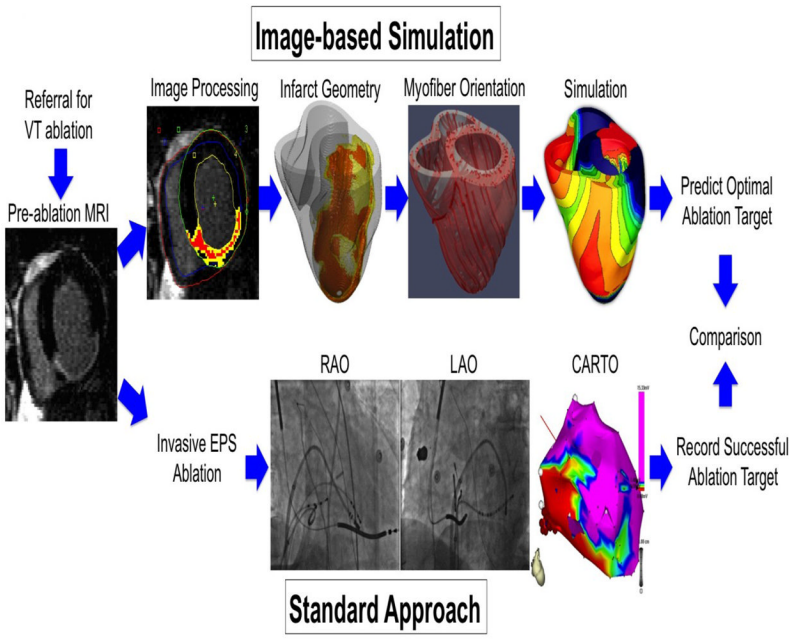

Figure 1. Study workflow

The patients referred for VT ablation (n=13) underwent pre-ablation MRI, which was processed to provide the heart and infarct geometry (red – scar, yellow - HZ), and estimated myofiber orientation *("Image-based Simulation").* These geometrical data were incorporated into mathematical simulation of VT to estimate potential target regions. Patients underwent an invasive electrophysiology study (EPS, n=13) and ablation *("Standard Approach",* n=11) using biplane X-ray fluoroscopy (RAO, right anterior oblique view; LAO, left anterior oblique view) and 3-D electroanatomical mapping (CARTO, Biosense Webster, Diamond Bar, California). Ablation lesion locations were recorded in 3-D space, and were compared with the target regions estimated by simulation. The study was retrospective but was conducted in a double-blind fashion, where the procedure operator was blinded to the simulation results, and the person who performed image processing and simulation was blinded to the clinical results.

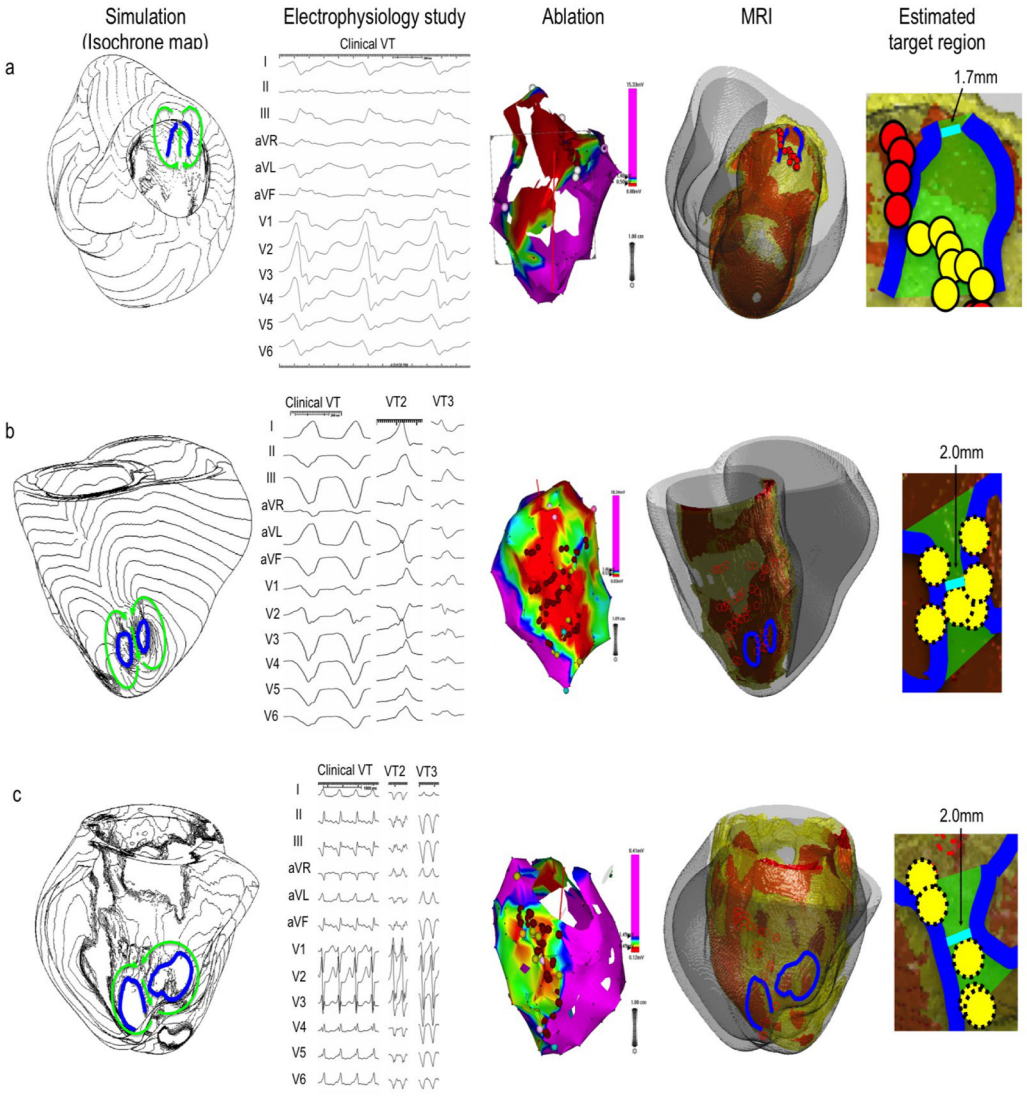

Figure 2. Comparison between image-based simulation and standard approach

Each row represents a different patient (a, b and c). The *Simulation* column shows VT with an isochrone map of activation based on image-based simulation. Green arrows indicate wave propagation of macro-reentry circuits. Lines of conduction block are indicated in blue. The *Electrophysiology study* (EPS) column shows the 12-lead electrocardiogram (ECG) of inducible VTs from the standard approach. The *Ablation* column shows the 3-D CARTO map with a color-coded voltage map (purple – normal myocardium, blue, green and yellow – infarct border zone, red – scar) from the standard approach. Red circles represent the ablation sites. The size of the circles does not reflect the size of ablation lesions. The *MRI* column shows pre-ablation MRI with infarct geometry (orange – scar, yellow – HZ, gray – non-infarct myocardium). The lines of conduction block (blue lines) from the image-based simulation and the ablation sites (red circles) from the standard approach are co-registered on the heart geometry. The *Estimated target region* column shows a potential target region (green area) estimated from the image-based simulation. The shortest possible line of ablation that spans the target region (i.e. narrowest width of the isthmus) is indicated in cyan. The ablation sites that fell within the estimated ablation target (green area) are indicated by yellow circles. All three simulation results in this figure (patient a, b and c)

show a figure-of-eight pattern, and are consistent with the 12-lead ECG of the clinical VT. The scales of the 12-lead ECG in the *Electrophysiology study* column is 100mm/s (patient a and b), and 25mm/s (patient c).

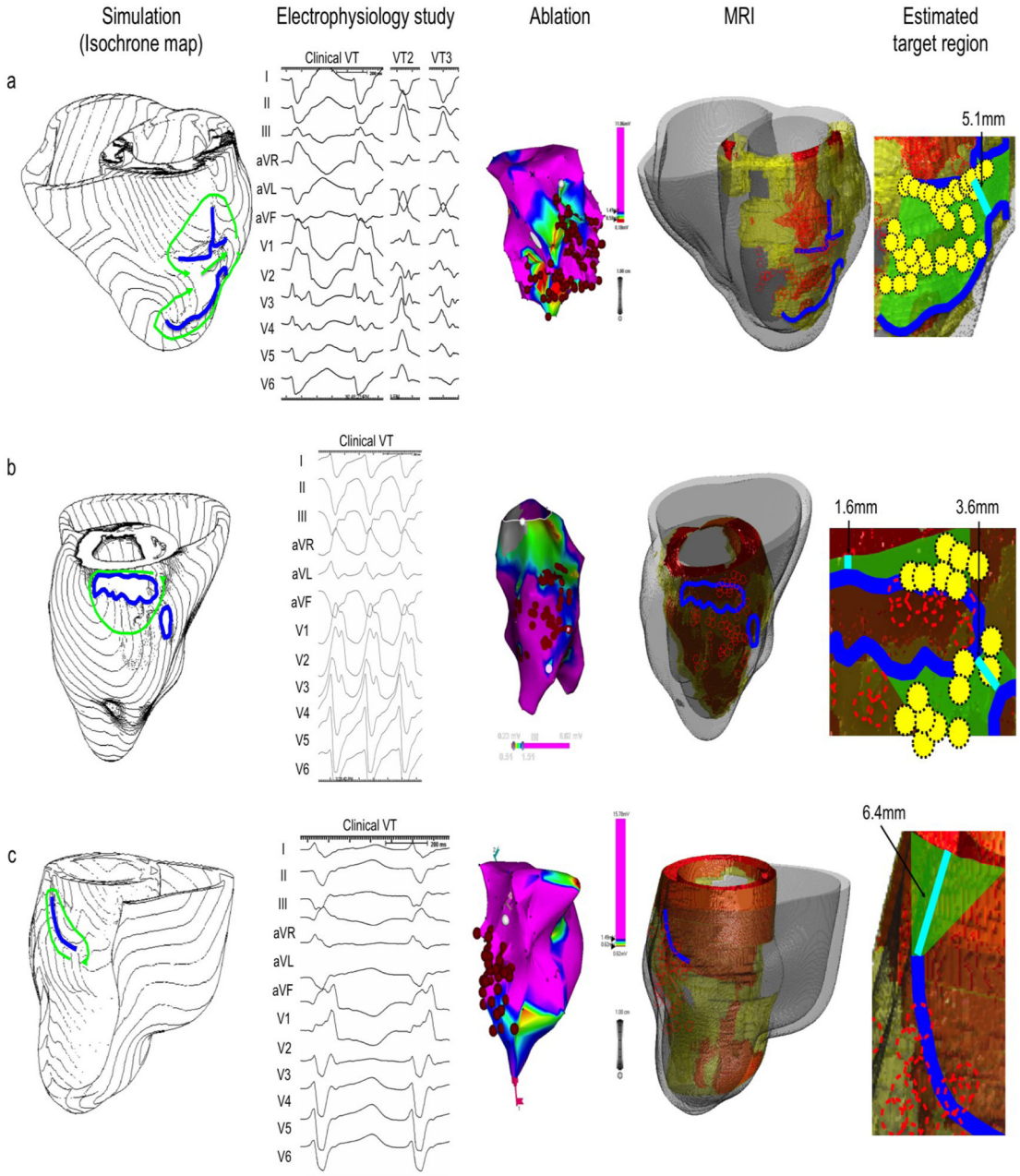

Figure 3. Comparison between image-based simulation and standard approach (continued)

The figure structure is the same as in Figure 2. The first two simulation results in this figure (patient a and b) show a figure-of-eight pattern, and the last simulation result (patient c) show a unidirectional circus movement pattern. All simulation results are consistent with the 12-lead ECG of the clinical VT. The scale of the 12-lead ECG in the *Electrophysiology study* column is 100mm/s (patient a, b and c).

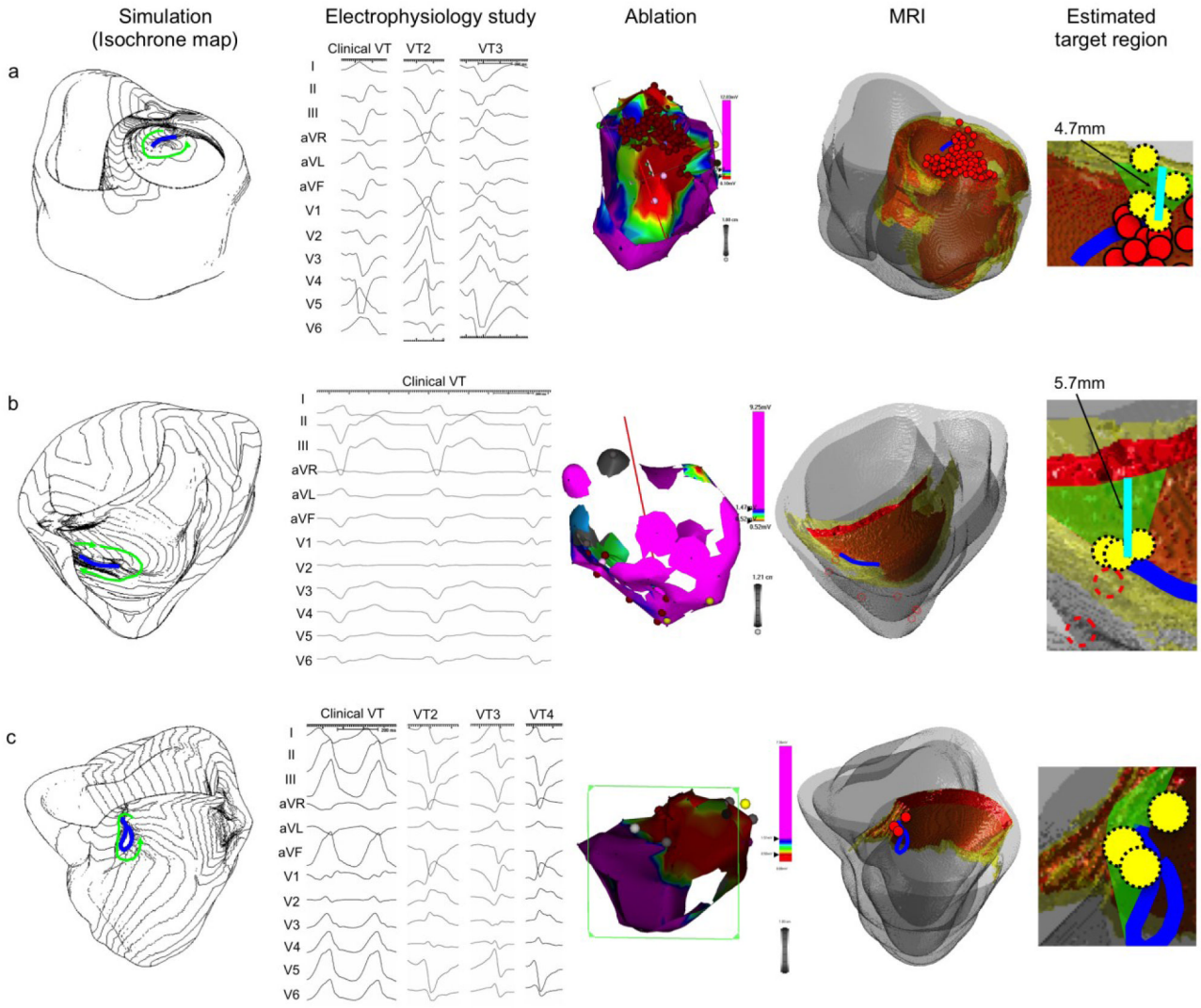

Figure 4. Comparison between image-based simulation and standard approach (continued)

The figure structure is the same as in Figure 2. All three simulation results in this figure (patient a, b and c) show a unidirectional circus movement pattern, and are consistent with the 12-lead ECG of the clinical VT. The scale of the 12-lead ECG in the *Electrophysiology study* column is 100mm/s (patient a, b and c).

Table 1

Baseline characteristics.

Patient	Figure	Age	Sex	Heart Disease	EF (%)	ICD	Scar	Clinical VT	Inducible VT
1	3a	68	M	CAD	60	No	Ant Sep Lat	1	3
2	Supp 1b	52	M	None	55	No	Inf	1	1
3	2a	71	M	CAD	35	No	Inf	1	1
4	4c	62	M	AR	55	No	Sep	1	4
5	Supp 1c	64	F	None	81	No	RV septum	1	1
6	4b	47	F	Sarcoidosis	34	No	Sep	1	1
7	2b	56	M	CAD	30	Yes	Inf	1	3
8	4a	72	M	CAD	29	No	Inf	1	3
9	2c	73	M	CAD	33	Yes	Inf Sep	1	3
10	Supp 1a	78	M	CAD	32	No	Ant Lat	1	1
11	Supp 2	66	M	CAD	31	No	Lat	1	1
12	3b	61	M	CAD	27	No	Inf Lat	1	1
13	3c	75	M	CAD	45	No	Sep Inf	1	1

EF, ejection fraction; ICD, implantable cardioverter-defibrillator; CAD, coronary artery disease; AR, aortic regurgitation; Ant, anterior wall; Sep, septal wall; Inf, inferior wall; Lat, lateral wall.

Table 2

Analysis of VT circuits and ablation

Patient	Figure	Image-Based Simulation		Standard Approach		Consistency
		Reentry pattern	Narrowest target width	Ablation in estimated target region	Acute success	
1	3a	Figure-of-eight	5.1 mm	Yes	Yes	Yes
2	Supp 1b	Circus movement	7.9 mm	N/A (EPS only)		
3	2a	Figure-of-eight	1.7 mm	Yes	Yes	Yes
4	4c	Circus movement	2.1 mm	Yes	Yes	Yes
5	Supp 1c	Noninducible		N/A	Yes	No
6	4b	Circus movement	5.7 mm	Yes	Yes	Yes
7	2b	Figure-of-eight	2.0 mm	Yes	Yes	Yes
8	4a	Circus movement	4.7 mm	Yes	Yes	Yes
9	2c	Figure-of-eight	2.0 mm	Yes	Yes	Yes
10	Supp 1a	Figure-of-eight	12.1 mm	N/A (EPS only)		
11	Supp 2	Circus movement	9.7 mm	No	No	Yes
12	3b	Circus movement	3.6 mm	Yes	Yes	Yes
			1.6 mm	Yes		
13	3c	Circus movement	6.4 mm	No	Yes	No
		Mean ± SD	5.0 ± 3.4 mm	9/11 = 82%	10/11 = 91%	9/11 = 82%